Eur. Phys. J. A (2023) 59:11
https://doi.org/10.1140/epja/s10050-023-00917-9

THE EUROPEAN PHYSICAL JOURNAL A

Regular Article - Experimental Physics

The resonances in the ^{22}Ne+α fusion reactions

M. Wiescher[a], **R. J. deBoer**[b], **J. Görres**

Department of Physics and Astronomy and the Joint Institute for Nuclear Astrophysics, University of Notre Dame, Notre Dame, IN 46556, USA

Received: 26 September 2022 / Accepted: 29 December 2022

Communicated by Nicolas Alamanos

Abstract The interplay and correlation between the ^{22}Ne(α, γ)^{26}Mg and the competing ^{22}Ne(α, n)^{25}Mg reaction plays an important role for the interpretation of the ^{22}Ne(α, n)^{25}Mg reaction as a neutron source in the s- and n-processes. This paper provides a summary and new data on the α-cluster and single-particle structure of the compound nucleus ^{26}Mg and the impact on the reaction rate of these two competing processes in stellar helium burning environments.

1 Introduction

Franz Käppeler was instrumental in the experimental and theoretical exploration of neutron capture reactions in the helium burning s-process environment as well in the identification and study of the two most likely neutron sources driving these processes at different environmental conditions, ^{13}C(α, n)^{16}O [1] and ^{22}Ne(α, n)^{25}Mg [2]. While the first reaction is better studied and understood over a wide energy range, especially in light of recent measurements [3], a multitude of questions remain associated with the nature and strength of the second neutron source. To address the issues of stellar neutron sources, the Notre Dame group has closely collaborated with the group of Franz Käppeler at the FZ Karlsruhe for nearly forty years. For this reason we will dedicate this article to the memory of Franz Käppeler and his contributions to this specific scientific question.

The ^{22}Ne(α, n)^{25}Mg reaction has been identified as the main neutron source for the weak s-process in the core helium burning environment of massive red giant stars [4], but it also plays an important role as the second neutron source for the main s-process during the helium flash in the hydrogen-helium intershell regions of AGB stars [2]. The reaction was also proposed as the main source for the n-process, which is triggered by the expanding supernova shockfront traversing through the helium burning shell of pre-supernova stars [5]. In all these cases the ^{22}Ne abundance in the helium enriched burning environment has been produced by a series of α capture reactions on the ^{14}N CNO ashes of the preceding hydrogen burning phase [6], ^{14}N(α, γ)^{18}F($\beta^+\nu$)^{18}O(α, γ)^{22}Ne. Because the reaction rates of ^{14}N(α, γ)^{18}F [7] and of ^{18}O(α, γ)^{22}Ne [8–11] are very fast, the initial ^{14}N material is rapidly converted into ^{22}Ne with the on-set of helium burning. The open question concerns the subsequent release of neutrons via the ^{22}Ne(α, n)^{25}Mg reaction. For this reason the reaction rate of the ^{22}Ne(α, n)^{25}Mg neutron source has been of great interest and a focus of many direct and indirect experimental, as well as theoretical, studies over the last 30 years [12–28].

The efficiency of the ^{22}Ne(α, n)^{25}Mg neutron source not only depends on the reaction rate at the specific temperature conditions of the s- or n-process sites, but also on the ^{22}Ne abundance in the stellar environment. It was pointed out in 1994 by [6] that the abundance of ^{22}Ne is strongly influenced by the rate of the competing ^{22}Ne(α, γ)^{26}Mg reaction. The ^{22}Ne(α, n)^{25}Mg reaction branch has a negative Q-value of $Q_{(\alpha,n)}$ = -478.34 ± 0.05 keV. This means the reaction channel for the neutron production opens only at higher temperature conditions. At lower temperature environments, during which the ^{22}Ne is being produced, the (α, n) channel remains closed and ^{22}Ne is not being processed further.

Typically the energy range of stellar burning for a reaction at a certain stellar environment with temperature T is estimated by the Gamow range $E_o \pm \Delta E$ given in units MeV

$$E_0 \pm \Delta E = 0.122 \cdot \left(Z_1^2 Z_2^2 \mu T_9^2\right)^{1/3} \pm 0.236 \cdot \left(Z_1^2 Z_2^2 \mu T_9^5\right)^{1/6}, \quad (1)$$

where Z_1 and Z_2 are the charge numbers of the interacting particles, μ the reduced mass of the interacting particles in amu and T_9 the stellar temperature in units 10^9 Kelvin. Nearby resonances outside the Gamow window may also

[a] e-mail: mwiesche@nd.edu (corresponding author)
[b] e-mail: rdeboer1@nd.edu

Published online: 30 January 2023

contribute to the reaction rate, depending on the resonance energy and resonance strength for both of the respective reaction branches. The Gamow range differs for the three environments where the ^{22}Ne(α, n) reaction is expected to play an important role as stellar neutron source.

For helium core burning in massive stars, only towards the very end of the burning phase, when the stellar helium core contracts towards higher densities and temperatures, does the neutron channel open and ignite the weak s-process. At these conditions the ^{22}Ne$(\alpha, n)^{25}$Mg reaction is considered the main neutron source. The main s-process, on the other hand, is driven primarily by the ^{13}C$(\alpha, n)^{16}$O reaction. However, with the on-set of the helium flash, causing a rapid increase in temperature in the hydrogen-helium intershell environment, the ^{22}Ne$(\alpha, n)^{25}$Mg reaction provides an additional neutron flux over the period of the actual helium flash. The idea of the n-process is associated with the ^{22}Ne abundance that has been built up during shell helium burning of massive stars. With the onset of the core-collapse supernova event and the emergence of the shock traversing through the helium burning shell, the material is rapidly compressed to high densities and temperatures, triggering the ^{22}Ne$(\alpha, n)^{25}$Mg neutron source and causing a high neutron flux for the n-process.

All three hot temperature scenarios are associated with a preceding cooler phase during which the ^{22}Ne can be depleted by the radiative capture ^{22}Ne$(\alpha, \gamma)^{26}$Mg reaction, which depends on the nuclear structure of the same ^{26}Mg compound nucleus and the strength of the γ channel. The ^{22}Ne$(\alpha, \gamma)^{26}$Mg reaction has a positive Q-value, $Q_{(\alpha,\gamma)}$ = 10614.74 ± 0.03 keV, and can contribute to the gradual depletion of ^{22}Ne at significantly lower temperatures than the ^{22}Ne$(\alpha, n)^{25}$Mg reaction, which is expected to dominate at temperatures between T = 0.1 and 0.6 GK, depending on the actual reaction rates [6,23,29,30].

2 The role of resonance strengths in the reaction rate

The rate of both the ^{22}Ne$(\alpha, n)^{25}$Mg and ^{22}Ne$(\alpha, \gamma)^{26}$Mg α capture processes depends entirely on contributions from single resonances, either as narrow resonance states within the temperature range of stellar burning, or as tail contributions from broad, higher energy states. Non-resonant contributions from $E1$ direct capture are forbidden and the influence of $M1$ and $E2$ direct capture is negligible compared to the resonance contributions. In general the reaction rate can be formulated as a sum of single resonance contributions, which depends critically on the resonance energies and strength of the contributing states, but for broader states, and the associated interference effects, one has to integrate numerically over the reaction cross section and Maxwell Boltzmann distribution of the interacting particles.

$$N_A\langle\sigma v\rangle = \left(\frac{8}{\pi\mu}\right)^{1/2} \frac{N_A}{(k_B T)^{3/2}} \int_0^\infty \sigma(E) E e^{-E/k_B T} dE, \tag{2}$$

where N_A is Avogadro's number, k_B is the Boltzmann constant, T is the temperature, and μ is the reduced mass.

For narrow and well separated resonances this formula can be simplified by numerical integration of the equation leading to the so-called narrow resonance formula:

$$N_A\langle\sigma v\rangle = 1.54 \cdot 10^{11} \frac{\mu}{T_9^{3/2}} \sum_i \omega\gamma_i \cdot e^{-11.605 \cdot E_r/T_9}, \tag{3}$$

which requires the determination of the resonance energies E_r in the center of mass system and the corresponding resonances strengths $\omega\gamma_i$ for the specific reaction channel(both in units [MeV]).

The ^{22}Ne$(\alpha, \gamma)^{26}$Mg reaction populates the ^{26}Mg compound nucleus at energies above E_x = 10.615 MeV. The neutron channel opens up at an excitation energy of E_x = 11.093 MeV. The reaction cross sections for both are characterized by a number of resonance states, with the resonance strengths determined by the different partial widths $\Gamma_{\alpha,\gamma,n}$, which depend on the underlying α- and single-particle structure component of the various excited states. This yields, for the strengths of resonances in the (α, γ) channel,

$$\omega\gamma_{(\alpha,\gamma)} = (2J+1) \cdot \frac{\Gamma_\alpha \cdot \Gamma_\gamma}{(\Gamma_\alpha + \Gamma_\gamma + \Gamma_n)} \tag{4}$$

and for the strength in the competing (α, n) channel:

$$\omega\gamma_{(\alpha,n)} = (2J+1) \cdot \frac{\Gamma_\alpha \cdot \Gamma_n}{(\Gamma_\alpha + \Gamma_\gamma + \Gamma_n)}, \tag{5}$$

where J is the spin of the compound nucleus state being populated.

For neutron bound states, Γ_n = 0, which contribute as low-energy (α, γ) resonances on the depletion of ^{22}Ne the resonance strengths are entirely determined by the α partial widths of the α unbound states. Because of the Coulomb barrier, these α widths are considerably smaller than the typical γ widths of the resonance states ($\Gamma_\alpha << \Gamma_\gamma$). In this case the resonance strength can be simplified to

$$\omega\gamma_{(\alpha,\gamma)} = (2J+1) \cdot \frac{\Gamma_\alpha \cdot \Gamma_\gamma}{(\Gamma_\alpha + \Gamma_\gamma)} = (2J+1) \cdot \Gamma_\alpha \tag{6}$$

Similarly for neutron unbound states with a substantial single-particle component the neutron width will be much larger than the γ width, which can be neglected. The neutron width will remain to be larger than the α width and the resonance strength will be

$$\omega\gamma_{(\alpha,n)} = (2J+1) \cdot \frac{\Gamma_\alpha \cdot \Gamma_n}{(\Gamma_\alpha + \Gamma_n)} = (2J+1) \cdot \Gamma_\alpha, \tag{7}$$

For excited states, above the neutron threshold, the situation is more complex when the γ- and neutron-widths

are comparable, while the α widths remain small due to the Coulomb barrier. In this case, an appreciable single-particle component in the wavefunction of the resonance state will play an important role. For pure α-cluster states, with a negligible single-particle contribution in the wave function, Γ_n remains very small and the strengths of the corresponding (α, n) and (α, γ) resonances depend on the strength of the single-particle channel with respect to the strength of the electromagnetic γ decay channel.

Except for cases where the neutron and γ decay channel is of comparable strength the ratio of the respective resonance strengths is determined by ratio of the decay probability into the the neutron or γ decay channel

$$\frac{\omega\gamma_{(\alpha,n)}}{\omega\gamma_{(\alpha,\gamma)}} = \frac{\Gamma_n}{\Gamma_\gamma}. \tag{8}$$

For levels with an appreciable single-particle component in the wavefunction, the neutron width will be larger than the γ width, with the corresponding resonance contributing to the (α, n) channel. For states with a negligible single-particle component, the corresponding resonances will still contribute to the (α, γ) channel however.

The role of the ^{22}Ne$(\alpha, n)^{25}$Mg reaction as a stellar neutron source therefore depends entirely on the quantum configuration of the α unbound states in the region of the α- and n-threshold in the compound nucleus ^{26}Mg. The level structure of ^{26}Mg at the corresponding high excitation energies, above $E_x > \approx 11$ MeV, is rather complex, which makes a reliable analysis of the actual resonance components somewhat daunting.

Previous attempts to derive a comprehensive analysis of the two reaction rates were based on Monte-Carlo analyses, incorporating all of the identified levels in the critical excitation range of nuclear burning with the various experimental and theoretical uncertainties in the resonance parameters [29,30] without detailed consideration of the underlying nuclear structure. The present approach aims at a comprehensive R-matrix analysis of the resonance parameters as identified by the different direct and indirect reaction studies of the various resonances. In the following sections we will discuss the α-cluster structure and the single-particle structure of the resonance components, respectively, in order to identify the states that contribute to the two reaction channels. The ^{22}Ne$(\alpha, n)^{25}$Mg reaction rate will be calculated by numerically integrating the measured cross sections over the Maxwell–Boltzmann distribution of the interacting particles for different temperatures. For the ^{22}Ne$(\alpha, \gamma)^{26}$Mg reaction, primary transition cross section measurements are very limited, and the approximation of narrow resonance strengths must still be used.

3 Nuclear structure considerations

For considerations of nuclear astrophysics, the level structure near the threshold of the entrance channel is of greatest relevance. Stars are low temperature environments where the critical energy range is given by the Gamow window which resembles approximately the shape of a Gaussian function with the center E_0 and width ΔE given by:

$$E_0 \pm \Delta E = 0.122 \cdot \left(Z_1^2 Z_2^2 \mu T_9^2\right)^{(1/3)} \pm 0.236 \cdot \left(Z_1^2 Z_2^2 \mu T_9^5\right)^{(1/6)}, \tag{9}$$

where Z_1 and Z_2 are the charge numbers of the interacting particles, μ is the reduced mass of the interacting particles and T_9 is the stellar temperature in units 10^9 Kelvin and the energy width of resonance states in the vicinity of the Gamow range [31]. The impact of the specific quantum configuration of such low-energy states near the threshold states is often neglected or treated as a random parameter in the determination of the level parameters and its contribution to the reaction rate. In cases such as the one of the ^{26}Mg compound nucleus considered here, the interplay between single-particle and α-cluster contributions for the neutron and α channel, respectively, plays an important role for evaluating and comparing the strength of the ^{22}Ne$(\alpha, n)^{25}$Mg and ^{22}Ne$(\alpha, \gamma)^{26}$Mg reaction channels. This aspect will be discussed in more detail in the following two sections to identify the resonances of impact for each channel.

3.1 The role of α-cluster structure in ^{26}Mg compound states

The level density in ^{26}Mg at high excitation energy is large and, in principle, many resonances may contribute as suggested in a recent analysis by [30]. However, strong selection rules are expected to substantially reduce the number of α induced resonances in the energy range of stellar burning. This is not only due to the fact that only natural parity levels can contribute as resonances [32], but also that only resonances with a pronounced α-cluster configuration will be able to contribute in a significant manner. According to the Ikeda rule [33], these kinds of states are anticipated to emerge near the α threshold as a collective phenomenon due to the strong coupling of bound states near the threshold to the continuum [34]. This would translate into a pronounced α strength and the corresponding resonances therefore may play a central role for the respective reaction rates.

In the present case, these contributions will be dominated by $J^\pi = 0^+$ and 1^- states because α particles with higher orbital momenta, populating higher spin states, will be suppressed by the orbital momentum barrier. Therefore only low-spin states will be considered. According to the discussion above, an important, and so far mostly neglected aspect, is the role of the single-particle component; α-cluster states with a considerable single-particle component contribute as

(α, n) resonances, while α-cluster states with a negligible single-particle component will emerge as (α, γ) resonances. All these selection rules need to be taken into account to identify the most important resonance states in the critical energy range of stellar burning [2]. For these reasons, only natural parity states with a pronounced α-cluster structure will contribute and we consider therefore only states which have been observed in α-transfer and scattering measurements such as by [23]. This approach differs from the recent analysis by [30], who included also levels observed in (p, p') and $(d.d')$ inelastic scattering studies in his considerations. These, however, are no indicator for natural parity or α-cluster level configurations and are therefore of only limited value for our considerations. In the energy range 10.65 MeV and 11.35 MeV 37 levels have been observed [19,35]. The recent (d, p) neutron-transfer study by [36,37] observed ten levels in this excitation range, which however, may be due to more limited resolution. The here chosen criterion suggests that only two or three states may contribute as pronounced cluster resonances in the low-energy range of the ^{22}Ne$(\alpha, n)^{25}$Mg reaction, while seven states can be expected to contribute as resonances to the low-energy range of the ^{22}Ne$(\alpha, \gamma)^{26}$Mg reaction. These states are listed in Table 1 with the excitation energies as well as spin and parities given in the most recent compilations. Based on these numbers we have adopted excitation energy as well as spin parity assignments for these states.

The most remarkable of these α-cluster states is located at an excitation energy of $E_x = 11.32$ MeV. It shows up as a strong resonance at about $E_{\mathrm{c.m.}} = 702$ keV in both reaction channels. This resonance dominates the reaction rate predictions for both channels, but there are discrepancies in the experimental data from direct studies and indirect measurements of the resonance components. Direct measurements [15,17,21] suggest an (α, n) resonance strength ranging between 83 ± 24 μeV, 118 ± 11 μeV, and 234 ± 77 μeV. On the other hand, the corresponding (α, γ) resonance strength is consistently measured to be at 37 ± 3 μeV [14,18,40,41]. This suggests that the γ channel has about 15% to 50% of the total strength.

Indirect studies of the decay of this level using the ^{22}Ne$(^6$Li$, d - \gamma)$ and the ^{22}Ne$(^6$Li$, d - n)$ reactions [25], however, suggest a comparable strength between the two decay modes. Normalizing to the (α, γ) resonance strength would translate into a substantially lower value for the (α, n) channel, significantly lowering the impact of this neutron source. This would represent a serious discrepancy between the results of the various experimental techniques. This could be due to errors in the efficiency of the neutron detection in the different direct ^{22}Ne$(\alpha, n)^{25}$Mg measurements, but this could also be the result of the limited resolution in the $(^6$Li$, d)$ studies. This might have influenced a reliable and accurate determination of the branching ratio. The previous discussion by [30] of the role of this state in stellar helium burning therefore seems premature until this discrepancy in the results of the different experimental approaches has been addressed. Angular distribution studies of α-transfer reactions suggest a $J^\pi = 0^+$ or 1^- spin and parity for the $E_x = 11.32$ MeV state and a recent ^{25}Mg(d, p) study [36] strongly supports the 1^- assignment. This assignment removes many of the uncertainties in the previous discussion of the resonance parameters of this level as discussed in more detail in Sect. 3.2.

A further question concerns possible contributions of lower energy resonances in both reaction channels. These again would be natural parity states, in order to satisfy the required selection rules. Such resonances are a challenge to measure directly because of their highly Coulomb-suppressed resonance strengths. For the same reason, only low spin resonances $J^\pi = 0^+, 1^-$ are expected to contribute in a significant manner. There have been a number of indirect attempts to identify and determine such low-energy α-unbound states below $E_x = 11.32$ MeV by [21–26]. Summarizing the different results, [24] highlights possible α unbound states in ^{26}Mg at $E_x = 11.17$ MeV, 11.08 MeV, and 10.95 MeV, corresponding to resonances at $E_{c.m.} = 557$, 466, and 334 keV, respectively.

Of particular interest for the reaction rate is the potential contribution of the $E_x = 11.17$ MeV state, which could result in a resonance at $E_{c.m.} = 557$ keV, providing a near threshold resonance decay into both reaction channels. This state has been identified in the ^{26}Mg(α, α') and ^{22}Ne$(^6$Li$, d)$ [23] reactions as a 1^- state based on an analysis of the angular distributions. The predicted resonance strength in the (α,γ) channel was $\omega\gamma_{(\alpha,\gamma)} = 0.54 \pm 7$ μeV.

A recent ^{22}Ne$(^6Li, d)$ α-transfer study by [25] suggested that the level may indeed decay into both the neutron and γ decay channel with seemingly comparable contributions. This analysis is, however, hampered by the limited resolution of the observed spectra. Contrary to that result, the recent sub-Coulomb ^{22}Ne$(^6$Li$, d)$ and ^{22}Ne$(^7$Li$, t)$ studies by [24] show no indication that this particular level is populated by α-transfer. This is a significant discrepancy. The $(^6$Li$, d)$ spectra taken at high ^{6}Li energies by [23] shows a clearly, and well separated, peak corresponding to this state, while the $(^6$Li$, d)$ and $(^7$Li$, t)$ spectra of [24], taken at energies below the Coulomb barrier, underline equally clearly the absence of such a transition. In addition, the α-transfer studies at medium ^{6}Li energies in inverse kinematics clearly show contributions of this level [25,26]. This discrepancy might be explained if this level has a high spin value, and the population by low-energy α-transfer is suppressed. Such a claim needs to be confirmed by directly mapping the excitation curve for this transition.

At lower energies the neutron bound states at excitation energies of $E_x = 11.08$ and 10.95 MeV are expected to contribute as resonances at $E_{c.m.} = 466$ and $E_{c.m.} = 334$ keV,

Table 1 Level parameters for suspected near threshold α-cluster states in the ^{26}Mg compound system from recent reaction studies.

^{22}Ne(^{6}Li,d) Talwar *et al.* (2016) [23]	^{26}Mg(α, α') Talwar et al. (2016) [23]		^{26}Mg(α, α') Adsley et al. (2017) [38]		^{26}Mg(d, d')/(p, p') Adsley et al. (2018) [35]		^{26}Mg(γ, γ') Longland et al. (2009) [39]		Adopted	
E_x (MeV)	E_x (MeV)	J$^\pi$	E_x (MeV)	J$^\pi$	E_x (MeV)	J$^\pi$	E_x (MeV)	J$^\pi$	E_x (MeV)	J$^\pi$
10.714 (20)	10.717(9)	1^-, 2^+	10.720 (9)		10.719 (2)	2^+			10.719 (2)	1^-
			10.806 (10)		10.806 (1)	1^-	10.8057 (7)	1^-	10.806 (1)	1^-
	10.822 (10)	0^+, 1^-	10.824 (10)	0^+	10.826 (1)	1^+			10.823 (1)	0^+
10.977 (20)	10.951(10)	1^-, 2^+	10.949 (10)	1^-	10.950 (1)	1^-	10.9491(8)	1^-	10.950 (1)	1^-
	11.085 (10)	2^+, 3^-	11.085 (10)		11.084 (1)				11.084 (1)	2^+
11.169 (17)	11.167 (8)	1^-, 2+	11.170 (10)		11.165 (1)	2^+			11.165 (1)	$\geq$1
11.317 (18)	11.317 (8)		11.290 (30)	≥ 1					11.318 (2)	1^-

respectively, to the ^{22}Ne(α, γ)^{26}Mg channel only. The predicted resonance strengths given by [21,23,24] depend on the α spectroscopic factor deduced from the respective transfer studies and seem to agree within an order of magnitude. The rather wide range of results obtained by these indirect studies might be caused by model dependent uncertainties in the analysis and differences in the adopted model parameters used for the extraction of the α spectroscopic factors of the two respective states. A higher accuracy would certainly be desirable, but a direct measurement of the two resonances remains a challenge. The spin and parity for both states, based on angular distribution measurements, range between $J^\pi = 0^+, 1^-$ and 2^+. Nuclear Resonance Fluorescence (NRF) studies [39] suggest a $J^\pi = 1^-$ assignment for the E_x = 10.95 MeV state, while a γ spectroscopy experiment [27] suggests a $J^\pi = 2^+$ assignment for the E_x = 11.084 MeV level. The uncertainties in these assignments translate directly into the uncertainty in the resonance strength and the contribution of these low-energy states to the ^{22}Ne(α, γ)^{26}Mg reaction rate. The α-transfer and scattering studies suggest a number of α unbound states at even lower excitation energies near the threshold listed in Table 1. These states may in principle contribute as weak resonances to the reaction rate but are located below the Gamow range so that their impact may be limited at the temperatures associated with the helium burning environment.

3.2 The single-particle component in ^{26}Mg compound states

The recent comprehensive analyses of the ^{22}Ne+α reaction channels by [30] took into account a ^{25}Mg(n, γ) radiative capture study by [19]. This latter study was based on a time-of-flight experiment at the n_ToF facility at CERN. Numerous resonances were observed in the ^{26}Mg compound nucleus, confirming the high level density of the quantum system at high excitation energies. Only a small subset of the observed states contribute to the ^{22}Ne+α reactions because of its particular selection rules.

A measurement of the ^{25}Mg(d, p) reaction should show a level distribution comparable to the resonance distribution in the radiative capture experiment. However, a recent study by [36] showed a much lower level density because reactions like ^{25}Mg(n, γ)^{26}Mg are mainly sensitive to s- and p-wave capture into J = 1, 2, 3, and 4 single-particle states with a pronounced γ strength. Neutron capture for higher ℓ value neutrons is reduced because of their reduced neutron penetrability through the orbital momentum barrier at near threshold energies.

On the other hand, the (d, p) reactions are limited in their sensitivity to the population of states with a pronounced single-particle structure. States with a small single-particle strength cannot be observed in a neutron-transfer reaction. There are in principle no limitations on ℓ-transfer and γ-strength. States observed in the (d, p) reaction can have a γ width that is too small to be observed as a neutron capture or also α capture resonance. In other words, the (d, p)-transfer reactions preferentially populate pronounced single-particle states, while radiative neutron capture resonances correspond to levels with dominant γ-decay strength. This phenomenon can be utilized for our discussion of the different decay channels of states populated by ^{22}Ne+α reactions.

The two neutron unbound states at E_x = 11.32 MeV and 11.17 MeV in ^{26}Mg are clearly observed in the ^{25}Mg(d, p) spectrum. For the state at E_x = 11.32 MeV, the angular distribution suggests an orbital-momentum-transfer of ℓ = 3. This would translate into spin-parity values of 1^- or 3^-. The latter assignment is unlikely because it would translate into a high orbital momentum barrier in the ^{22}Ne+α channel, incompatible with the observed resonance strengths. The level has not been observed as a resonance in the ^{25}Mg(n, γ) experiment by [19], which suggests a very small single-particle component. This confirms the argument that the neutron partial width Γ_n should be comparable to the γ partial width

Table 2 Partial width predictions for states near the neutron threshold in the ^{26}Mg compound system

E_x (MeV)	$E_{c.m.}$ (MeV)	J^π	Talwar et al. (2016) [23] Γ_α (eV)	Ota et al. (2021) [26] Γ_α (eV)	Jayatissa et al. (2020) [24] Γ_α (eV)	Adsley et al. (2018) [35] Γ_α (eV)	Γ_γ (eV)	Γ_n (eV)
10.719	0.104	1^-	2.5×10^{-36}					
10.950	0.336	1^-	6.7×10^{-14}	3.00×10^{-14}	3.00×10^{-14}			–
11.085	0.471	2^+	$\leq 8.4\times10^{-12}$	5.70×10^{-11}	5.70×10^{-11}	5.70×10^{-11}	3[a]	–
11.165	0.551	4^+	$< 1.3\times10^{-11}$					$\Gamma_n < 0.1\ \Gamma_\gamma$
		2^+	1.00×10^{-7}	$<1.3\times10^{-11}$				$\Gamma_n < 0.1\ \Gamma_\gamma$ [c]
11.320	0.702	1^-	5.00×10^{-5}	3.00×10^{-5}	1.30×10^{-5}	2.70×10^{-5}	0.4-1.0[b]	1.3[d]

[a] An estimate made by [28]
[b] Calculated range found using Γ_n from [36] and Γ_n/Γ_γ from direct measurements and from that of [25]
[c] See Refs. [17,23]
[d] See Ref. [36]

Γ_γ. DWBA analysis yields a value of $(2J+1)\Gamma_n = 3.9$ eV. This translates into a neutron width of 1.3 eV for the 1^- spin assignment. That is barely within the sensitivity limit of the ^{25}Mg(n,γ) study and explains why this specific state was only weakly observed. The analysis of the ^{25}Mg(n,γ) resonance yields a γ width of about 5±4 eV, which is not sufficiently accurate to make a conclusion about the relative strengths of the neutron and γ decay channels.

The evaluation of the $E_x = 11.17$ MeV state contributing to the ^{22}Ne+α reaction branches is rather complex, because, in previous studies, there have been three neutron unbound levels identified in this energy range. This makes a unique assignment and comparison of resonance parameters nearly impossible. The excitation energies of these levels are not sufficiently well known to identify which transfer or capture reaction populates which one of the assembly of unbound states.

The R-matrix analysis of the (n,γ) data by [19] suggests two states at $E_x = 11.163$ (2^+) and 11.169 (3^-) MeV, both having a neutron width in the keV range. A third state is at $E_x = 11.171$ MeV, with a γ width of 5±1 eV and a neutron width of 1–30 eV.

The angular distribution of the (d,p) single-particle transition to the $E_x = 11.165$ MeV state in [36] excludes an $\ell = 0$ transfer. The best fit suggests $\ell = 1$; excluding a 2^+ assignment, we therefore suggest that this state most likely corresponds to the 3^- state identified by [19].

The $E_x = 11.171$ state was neither observed in the (d,p)-transfer experiment by [36], nor in the (n,γ) study by [19], suggesting a very small neutron width. We identify this state as the ^{22}Ne+α resonance state observed in the $(^6$Li$,d)$ and (α,α') studies by [23]. Given the upper limit for the (α,n) strength given by [17], indeed requires a small neutron width in the eV range. While the ^{22}Ne$(^6$Li$,d)$ transfer studies by [25] at medium energies also shows indications for this level, the sub-Coulomb transfer measurement by [24] has no indication of this particular level at $E_x = 11.17$ MeV and the upper limit for the resonance strength would be in the range of $\omega\gamma_{(\alpha,\gamma)} = 0.006$ μeV. This has been interpreted as an indication for a higher spin parity assignment than suggested by [23]. Inelastic scattering (d,d') and (p,p') studies populating this level are still consistent with a spin of 4^+, but higher spins are unlikely to be observed in light particle scattering. Following [35] we adopt an excitation energy of 11.165 MeV and list the partial widths for this state for the possible 2^+ and 4^+ assignments in Table 2.

4 Resonance strengths in ^{22}Ne$(\alpha,n)^{25}$Mg and ^{22}Ne$(\alpha,\gamma)^{26}$Mg

The amplitude of the α-cluster and single-particle configurations of the α-unbound states near the threshold determine the strengths of the various resonances in the two reaction channels as discussed in the previous section. In the following section we will discuss the present status and uncertainties associated with the resonance strengths and the impact on the reaction rates.

We will first focus primarily on the narrow resonances. The neutron unbound states with fairly large neutron widths in the keV range will be discussed in Sect. 5. In the case of the aforementioned narrow resonance at $E_{\rm c.m.} = 702$ keV, associated with the level $E_x = 11.32$ MeV in the ^{26}Mg compound nucleus, the critical issue for the resonance strength is the comparison between the (α,n) and the (α,γ) channels, which determine the efficiency of the ^{22}Ne$(\alpha,n)^{25}$Mg reaction as a neutron source in high temperature environments as outlined in Sect. 1. The ratio of the resonance strengths equals the ratio of the neutron partial width Γ_n of the state over its γ partial width Γ_γ as defined in Eq. 8.

As mentioned before (see Sect. 2), [24] had derived a ratio of $\Gamma_n/\Gamma_\gamma = 1.14(26)$, suggesting that the (α,γ)

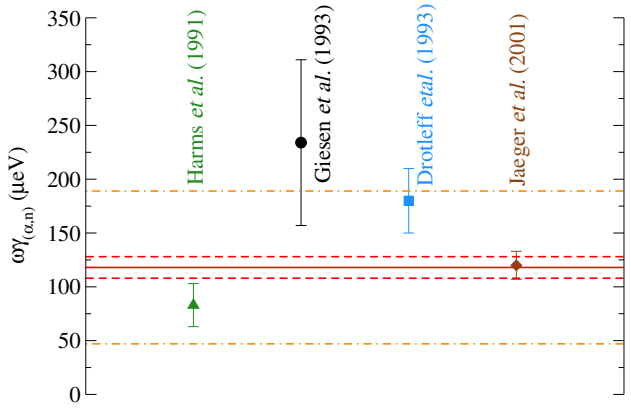

Fig. 1 Comparison of $\omega\gamma_{(\alpha,n)}$ for the $E_{\text{c.m.}}$ = 702 keV resonance in the ^{22}Ne$(\alpha, n)^{25}$Mg reaction

and the (α, n) reaction strengths are about equal. This disagrees with a series of independent direct resonant capture studies of this state, which indicate a substantially higher neutron branching. The four measurements of the resonance strength of ^{22}Ne$(\alpha, n)^{25}$Mg have been performed independently by [15–17,21] using different target and neutron detection techniques, the results vary, but are consistent within the error bars with a weighted mean value of $\omega\gamma_{(\alpha,n)} = 118 \pm 10_{\text{stat}} \pm 71_{\text{syst}}$ μeV, with statistical and systematic uncertainties accounted for separately. The deviations between the values are primarily due the systematic uncertainties.

The resonance strength, $\omega\gamma_{(\alpha,n)} = 234 \pm 77$ μeV given by [21] is based on an experiment with an implanted ^{22}Ne target. Within the given uncertainties this value is in fair agreement with the strength, $\omega\gamma_{(\alpha,n)} = 180 \pm 30$ μeV, obtained by an extended gas target measurement [16]; a subsequent gas target measurement with "improved detector sensitivity", however yields a substantially lower value, 120 ± 13 μeV [17]. The measurement by [15] also gives a very low value for the resonance strength of $\omega\gamma_{(\alpha,n)} = 83 \pm 20$ μeV with 1 σ uncertainty. This value, however, was not obtained in a direct experiment because of the low efficiency of the ^{3}He spectrometers, but was estimated from comparison with the data observed by [14]. A comparison of the resonance strengths is given in Fig. 1.

The differences in target and detector arrangements between all these experiments, cause the spread in data and the relatively large systematic errors. However the data points overlap within the range of the given uncertainties and are systematically higher than the average value for the resonance strength in the competing ^{22}Ne$(\alpha, \gamma)^{26}$Mg channel $\omega\gamma_{(\alpha,\gamma)} = 37 \pm 5$ μeV as measured by [14,18] and more recently by [41]. This difference in strength of the (α, n) and (α, γ) channel is clearly discrepant with the claim of a comparable strength for both channels by [24]. The limited resolution in their (^{6}Li, d) study of 230 keV, may have inhibited a clear identification and resolution of the populated excited states, which might have influenced the determination of the branching ratio.

This discrepancy cannot be addressed in the framework of the existing data and has to await the results of a recent ^{22}Ne$(\alpha, n)^{25}$Mg measurement, which was performed at the CASPAR underground accelerator and is presently being analyzed.

No direct measurements of resonance strengths are available for the lower unbound excited states. The resonance strengths of the states in the different reaction channels depend on the partial width in the α, neutron, and γ channels as outlined above. The partial widths used in this work have been deduced from a number of indirect studies [23,35,38] complemented by additional information from neutron capture [19] and neutron-transfer measurements [36]. Of great interest is the resonance corresponding to the neutron unbound state at 11.17 MeV. This level has been identified as a potential 1^- by state [23] but the recent α-transfer studies by [24,26] indicate that the cross section for the α-transfer depends sensitively on the beam energy and cannot be observed at sub-Coulomb energy. This suggests that the state at 11.17 MeV most likely corresponds to a higher spin value. Because of the close vicinity of other levels [19] it is very possible that the different transfer reaction studies are also handicapped by populating nearby unresolved states in that excitation range. Indeed, recent direct radiative α capture measurements by [41] only obtained an upper limit for the resonance strength that is inconsistent with the value suggested by [23]. We therefore conclude that the existence of a lower energy ^{22}Ne(α, γ) resonance is unlikely contrary to earlier claims [23]

Lower-energy α-unbound states are all neutron bound and therefore may only contribute to the ^{22}Ne(α, γ) reaction channel. For our considerations, we include only the ones characterized by a pronounced α-cluster structure reflected in the strong population of the levels in α-transfer and inelastic α scattering. The results are listed in table 3, comparing the results of the recent evaluation by [30] and the results by [23] modified by small changes in the energy assignment of the resonance states based on higher resolution experiments [36,37].

The 2^+ resonance level a $E_x = 11.085(1)$ MeV has been observed in α-transfer and α inelastic scattering studies [23,38]. The corresponding resonance at $E_{\text{c.m.}} = 471$ keV is just below the neutron-threshold ($S_n = 11.093$ MeV) and is expected to only contribute to the (α, γ) reaction channel. The listed resonance strengths are consistent with each other. The predicted strength of the 1^- resonance at $E_{\text{c.m.}} = 335$ keV ($E_x = 10.950(1)$ MeV) is solely based on the data provided by [23]. The assumptions about the α spectroscopic factor [22] made in the former evaluations [29,30] have not

Table 3 Resonance strengths for the ^{22}Ne(α, γ)^{26}Mg and the ^{22}Ne(α, n)^{25}Mg reactions at energies below 1 MeV

E_x (MeV)	$E_R^{c.m.}$ (MeV)	J^π	[30] $\omega\gamma_{(\alpha,\gamma)}$ (eV)	[30] $\omega\gamma_{(\alpha,n)}$ (eV)	[23] $\omega\gamma_{(\alpha,\gamma)}$ (eV)	[23] $\omega\gamma_{(\alpha,n)}$ (eV)
10.719 (2)	0.104	1^-			$2.4^{+4.6}_{-1.6} \times 10^{-35}$	
10.950 (1)	0.335	1^-			$2(1)\times10^{-13}$	
11.085 (1)	0.471	2^+	2.85×10^{-10}		$\leq 4.2\times19^{-10}$	
11.320 (2)	0.702	1^-	$3.7(4)\times10^{-5}$	$4.2(11)\times10^{-5}$	$3.5(4)\times10^{-5}$	$1.2(4)\times10^{-4}$

The data of reference [23] depend on ^{22}Ne(^6Li, d)^{26}Mg transfer studies except for the state at E_x = 11.32 MeV, which is based on direct measurements. The low-energy resonance data of [30] takes additional proton and deuteron induced reaction studies into account. The resonance strength associated with the E_x = 11.32 MeV relies on transfer studies by [24,26]. For this table only resonances with an appreciable strength have been considered

been confirmed. The level has also been observed in inelastic ^{26}Mg(α, α') scattering [38], but no estimate for the resonance strength has been given.

A very low-energy resonance at $E_{\text{c.m.}}$ = 104 keV (E_x = 10.719(2) MeV) is included in the Table 3 [23]. Angular distribution measurements suggests either a 1^- or 2^+ spin and parity assignment. The resonance strength is too low to make a contribution to the reaction rate.

5 Rate of the ^{22}Ne(α, n)^{25}Mg reaction

The most recent calculations of the reaction rate have been done using resonance strengths and the narrow resonance approximation [29]. For low energies, where no experimental data exist, this method may be valid, as the resonances that are thought to contribute substantially to the reaction rate are very narrow. However, at higher energies the cross section is well measured and has been shown to be composed of broad overlapping resonances, not narrow isolated ones. Therefore, it seems more appropriate for the reaction rate to be calculated by numerically integrating the well-mapped experimental cross sections where available. This also has implications for the way in which the uncertainties should be interpreted.

5.1 ^{22}Ne(α, n)^{25}Mg at $T \gtrsim 0.3$ GK

The rate of the ^{22}Ne(α, n)^{25}Mg reaction around 0.3 GK can be calculated via direct numerical integration of the experimental cross sections for $E_\alpha \geq$800 keV in the center of mass system. The data of [13,16,17], which are largely consistent with each other in overlapping energy regions, cover the energy range $0.693 < E_{\text{c.m.}} < 4.34$ MeV. Statistical model calculations from the Hauser–Feshbach (HF) code SAPPHIRE [42] are used to estimate the cross section up to $E_{\text{c.m.}}$ = 18 MeV. This allows for direct calculation of the reaction rate by this method in the temperature range

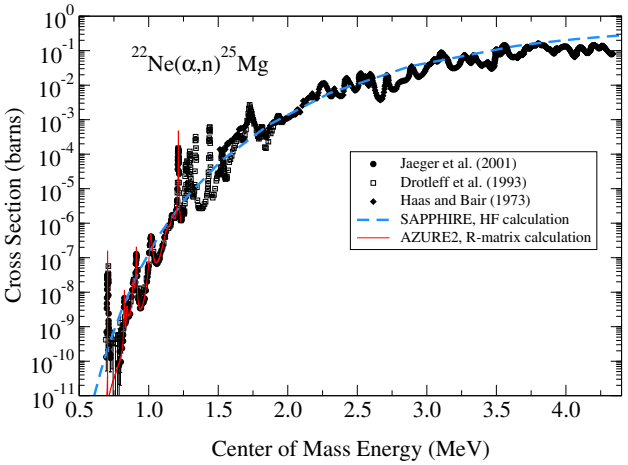

Fig. 2 Experimental cross sections by Jaeger et al. [17], Drotleff et al. [16], and Haas et al. [13]. An R-matrix calculation of the cross section, over the region of the data of [17], is indicated by the solid red line while an HF calculation, over the entire energy range (which extends up to $E_{\text{c.m.}}$ = 18 MeV), is indicated by the dashed blue line

$0.3 < T < 10$ GK. The cross section data are shown in Fig. 2.

The measurements of [15] also report excitation functions that overlap with the energy ranges of [16,17]. These measurements report partial cross sections of the ^{22}Ne(α, n)^{25}Mg reaction through measurements of the prompt neutrons using ionization chambers, providing a means of high resolution neutron spectroscopy. However, the cost to efficiency from this type of experimental setup required the use of thicker targets, resulting in considerable energy broadening.

At α energies above E_{cm} = 1.06 MeV additional neutron channels are opening up populating excited states in ^{25}Mg. The measurements of [15] have the significant advantage that the neutron energies are known, and thus there is no ambiguity in the efficiency. This is not the case for the measurements of [16], where their counter thermalizes the neutrons and all neutron energy information is lost. This issue with neutron counter type detectors has been highlighted recently for the ^{13}C(α, n)^{16}O reaction [43].

The total cross section curve of [16] and the excitation functions of [15] were normalized, numerically integrated to obtain the partial rates, and summed to obtain the total rate. This was then compared to the rate obtained with the data from [16], and was found to agree to with in ≈10%. Therefore, for the remainder of this work the data of [16] was used.

Within the experimental range, the total uncertainty is dominated by the common-mode (systematic) uncertainty in the absolute cross section for each measurement under consideration. Only the experimental data of [13] give a clear statement of their systematic uncertainty, which is quoted as 12%. From the uncertainties in the resonance strengths of [16], their systematic uncertainty was ≈11%. Resonance strength uncertainties in [17] are as small as 4%, which seem to not take into account, or grossly underestimate, systematic uncertainties of the target thickness and neutron detection efficiency. This type of uncertainty underestimation has been shown to be an issue for similar measurements of the $^{13}C(\alpha, n)^{16}O$ reaction [43].

As the data of [17] overlap with those of [16] who in turn overlap with [13] as shown on Fig. 2, the level of agreement in both the energy dependence and absolute cross sections of the different data sets can be easily compared. The data of [16,17] are found to be in good agreement in both respects. The data of [13,16] show some discrepancy in both shape and absolute scale. Much of the difference in shape appears to be the result of rather different target thicknesses and levels of background. It is estimated that the data of [13] should be reduced by ≈25% in order to be more consistent with the data of [16].

The average cross section calculated using the Hauser-Feshbach model with the code SAPPHIRE agrees reasonably well with the average cross section of the data of [16,17]. However, the HF calculation tends to over predict the data of [13] above $E_{\text{c.m.}} = 2.9$ MeV by about 20%, or a 40% over prediction when normalized to the data of [16]. The reaction rate obtained using the SAPPHIRE code agrees to within 10% with the high temperature ($T > 2.5$ GK) rate of [29].

While the cross section at higher energies is dominated by broad resonance structures, i.e. with widths that are much larger than the energy loss through the targets used by the experimental studies. In order to more accurately calculate the rate over this energy region, an R-matrix fit [44,45] was performed to the data of [17], which included an experimental target thickness correction. The R-matrix cross section, free of the resolution correction, was then used for the numerical integration. The R-matrix fit to the S-factor of the $^{22}Ne(\alpha, n)^{25}Mg$ reaction data by [17] after target thickness correction is shown in Fig. 3. At higher energies, it becomes energetically possible for the $^{22}Ne(\alpha, n)^{25}Mg$ reaction to populate excited final states in ^{25}Mg, greatly complicating the R-matrix analysis. However, in conjunction with

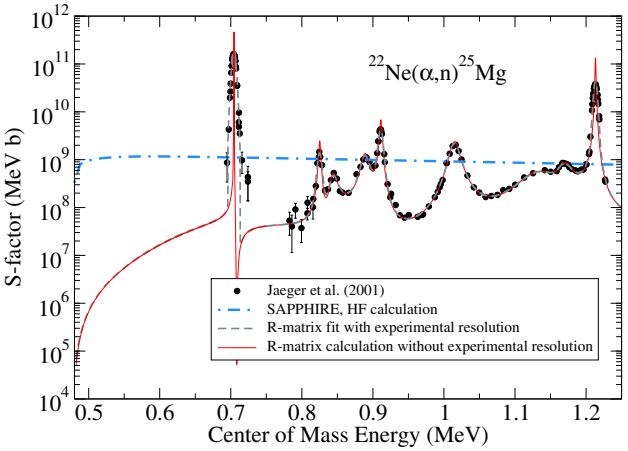

Fig. 3 R-matrix calculation from a fit to the experimental $^{22}Ne(\alpha, n)^{25}Mg$ data of Jaeger et al. [17] (black points). The R-matrix S-factor, without (with) experimental resolution correction, is indicated by the red solid line (grey dashed line). A SAPPHIRE HF calculation is shown for comparison (blue dashed-dotted line)

the $^{22}Ne(\alpha, \gamma)^{26}Mg$ data, the partial cross section data of [15] are fit, as described in Sect. 5.2.

Figure 4 shows the ratio of the reaction rate calculated by direct numerical integration as described above to the median rate of [29]. Significant differences are observed in both the uncertainty and the median values of the reaction rates. In the present work, an energy independent (or temperature independent) uncertainty of 15% has been adopted based on the systematic uncertainties of the experimental cross section curves. In [29], resonance strengths with varying uncertainties were used, mostly from [17]. However, in [17] the cross section data were fitted as a sequence of non-interfering but overlapping and Breit–Wigner resonances, which actually should be strongly correlated. Thus the uncertainties quoted in [29] cannot be treated as independent parameters and many of the resonance strength uncertainties are greatly underestimated. This leads to a significant underestimation of the reaction rate uncertainty at temperatures above ≈ 0.6 GK.

The differences in the central value of the present rate compared to that of [29] comes mainly from the energy (or temperature) where the rate calculations switch over from isolated resonance or direct integration of the experimental data to a statistical HF cross section. In [29], the effective thermonuclear energy range of [46] was used to determine the cut off temperature at which experimental resonance data should be replaced with an HF calculation. While this method may be a good general method, in the case of the $^{22}Ne(\alpha, n)^{25}Mg$ reaction, there exists accurate total cross section data up to quite high energies [13,16]. In Fig. 4, the increase in the reaction rate of this work over that of [29] at $T \approx 1$ GK comes from the inclusion of the cluster of strong, narrow, resonances observed in the data of [16], at just higher energies than the data of [17], between $1.23 < E_{\text{c.m.}} < 1.46$ MeV. At higher

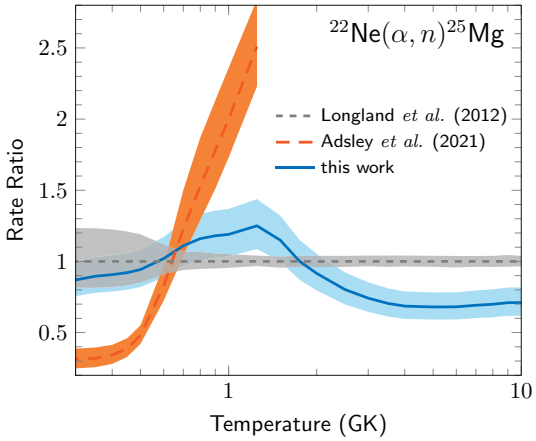

Fig. 4 The ^{22}Ne$(\alpha, n)^{25}$Mg reaction rate of this work and that of Adsley et al. [30] relative to the median value of Longland al. [29]. The median value of this work is indicated by the blue solid line, while the estimated 15% uncertainty band is indicated by the blue shaded region. The median value of Adsley et al. [30] (with Texas A&M results) is indicated by the orange long dashed line while the associated uncertainty is indicated by the shaded orange region. The uncertainty band of [29] is indicated by the gray shaded region. See text for details

temperatures ($T > 2$ GK), the reduction in the rate comes from the use of the data of [13] as described above, which are systematically lower than the HF calculations by $\approx$ 20-30%.

There is also a significant difference of the reaction rate presented here at high temperatures compared to that of [29]. This stems directly from the underestimation of the strength uncertainties in [17], which were then used by [29]. For example, the highest energy, strong, resonance at $E_\alpha = 1434$ keV observed by [17] has an uncertainty in its strength of $\approx 4\%$, which is essentially the uncertainty in the reaction rate of [29] at $T > 1$ GK. This same uncertainty seems to have been adopted for the HF portion of the reaction rate as well. This seems rather optimistic considering that the higher energy data of [13,16] continue to show clear resonance structures in the cross section up to their highest energies.

5.2 ^{22}Ne$(\alpha, n)^{25}$Mg at temperatures $T \lesssim 0.3$ GK

In the low temperature region, below the lowest observed resonance at $E_{\text{c.m.}} = 702(2)$ keV, corresponding to the state at $E_x = 11.318(2)$ MeV and above the neutron separation energy at $S_n = 11.09308(4)$ MeV [47,48], the reaction rate is determined from energies and partial widths from indirect studies. There have been many levels observed over this excitation energy region, but α-transfer reactions indicated that only a single level is present in this region with a large α-particle strength at $E_x = 11.165$ MeV ($E_{\text{c.m.}} = 551$ keV) (see Table 2). From the upper limits on the ^{22}Ne$(\alpha, n)^{25}$Mg cross section measured by [17], the upper limit on the strength for this resonance is $\omega\gamma_{(\alpha,n)} < 6\times10^{-8}$ eV.

6 Rate of the ^{22}Ne$(\alpha, \gamma)^{26}$Mg reaction

There are only a few studies of the ^{22}Ne$(\alpha, \gamma)^{26}$Mg reaction. The resonance pattern follows at higher energies the pattern of the competing ^{22}Ne$(\alpha, n)^{25}$Mg reaction as reflected by the excitation curve studied by [14] in the energy range 800 keV $< E_\alpha <$ 2.2 MeV. This excitation curve is based on the transition of the first excited state ($J^\pi = 2^+$) at $E_x = 1.809$ MeV to the ground state. Most of the reaction strength is assumed to be in that transition since resonances decay primarily as cascades to this state and then to the ground state. The cross section does not reflect a possible direct capture to the ground state of ^{26}Mg, but this transition is largely suppressed in α capture by the effective charge factor of 0.045 and expected to be negligible compared to the contributions of the overlapping broad resonances [8]. The resonance strengths of the levels between 1.4 and 2.05 MeV α-energy, documented in Table 1 of [14], are substantially smaller than the strengths of the resonances in the competing (α, n) reaction channel. However, at lower energies the strength of the $E_\alpha = 830$ keV resonance is comparable to the strength of the resonance in the competing ^{22}Ne$(\alpha, n)^{25}$Mg reaction channel as mentioned before. This resonance dominates the rate at temperatures between 0.25 and 1.0 GK, and thus has seen special additional attention in subsequent publications by [18] and more recently by [41]. Unpublished results can also be found in [40], which confirm the strength.

In a similar manner to the ^{22}Ne$(\alpha, n)^{25}$Mg reaction, the ^{22}Ne$(\alpha, \gamma)^{26}$Mg rate is calculated utilizing the single narrow resonance approach for the energy range up to $E_{\text{c.m.}} \approx 1.2$ MeV. For the range from 1.2 $< E_{\text{c.m.}} <$ 1.8 MeV an R-matrix fit to the data of [14,40] is used, which was fit simultaneously to the partial ^{22}Ne$(\alpha, n_{0,1,2})^{25}$Mg cross sections of [15], as shown in Fig. 5. At higher energies, the rate was calculated using the HF cross section from the SAPPHIRE code. The components were summed to determine the total reaction rate for the ^{22}Ne$(\alpha, \gamma)^{26}$Mg over the entire temperature range.

6.1 ^{22}Ne$(\alpha, \gamma)^{26}$Mg at temperatures $T \gtrsim 1$ GK

The R-matrix analysis for the observed resonance features in ^{22}Ne$(\alpha, \gamma)^{26}$Mg for energies 1.2 $< E_{\text{c.m.}} <$ 1.8 MeV is based on the experimental data provided by [14,40] for the γ transition from the first excited state to the ground state. Detailed decay branchings have not been determined, but similar to what has been reported for the ^{18}O$(\alpha, \gamma)^{22}$O reaction [8], the results by [14] suggest that a direct ground state transition is expected to be small, with between 84 and 98% of the ^{22}Ne$(\alpha, \gamma)^{26}$Mg strength as reflected in the secondary γ-ray decay from the first excited state to the ground state. Figure 5 shows the R-matrix fit for the secondary transition from the first excited to ground state compared to the fit

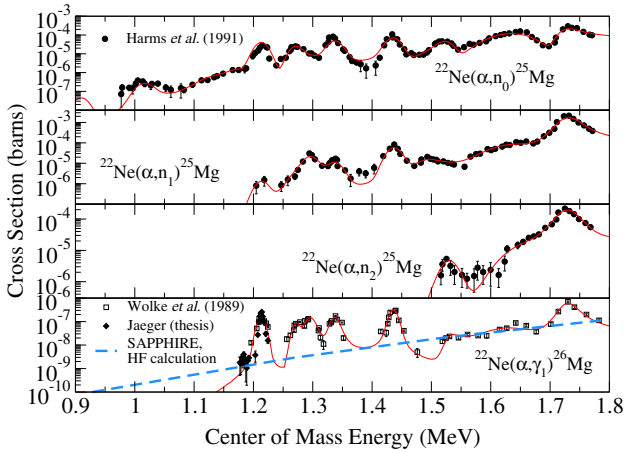

Fig. 5 The R-matrix fit to the ^{22}Ne(α, $n_{0,1,2}$)^{25}Mg data of Harms et al. [15] and the ^{22}Ne(α, γ_1)^{26}Mg data of Wolke et al. [14] and the PhD thesis of Jaeger [40]. The red line indicates the R-matrix cross section convoluted with the experimental resolution to reproduce the experimental yields

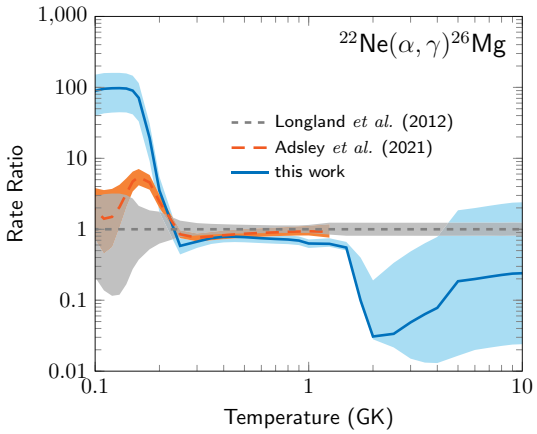

Fig. 6 The ^{22}Ne(α, γ)^{26}Mg reaction rate relative to the median value of Longland et al. [29]. The median value of this work is indicated by the blue solid line, while the estimated uncertainty band is indicated by the blue shaded region. The median value of Adsley et al. [30] (with Texas A&M results) is indicated by the long dashed orange line, while their reported uncertainty is indicated by the shaded orange region. The uncertainty band of Longland et al. [29] is indicated by the gray shaded region. See text for details

of the ^{22}Ne(α, n)^{25}Mg data by [15]. Despite the rather high level density, the resonances populated in ^{22}Ne(α, γ)^{26}Mg and ^{22}Ne(α, n)^{25}Mg reaction channels seem to be the same, greatly facilitating the R-matrix description of the data. There are some regions where the R-matrix fit somewhat poorly describes the experimental data, which is likely a combined result of only an approximate modeling of the experimental resolution, contributions from weaker underlying states, and incorrect interference resulting from incorrect J^π assignments.

The uncertainty of the [14] data are dominated by the overall systematic uncertainty, 9%, and the uncertainty in the contribution of the ground state transition. Therefore, a 9% uncertainty is adopted for the lower uncertainty of this data while a 20% uncertainty is adopted for the upper uncertainty. At higher energies, the only data available is that of [49].

Based on a comparison of the data of [14,49] with the HF cross section calculated from the SAPPHIRE code, an uncertainty of an order of magnitude is estimated. Similar to the ^{22}Ne(α, n)^{25}Mg reaction rate calculation described in Sect. 5, the present rate differs substantially from that of [29] above $\approx$ 2 GK because the present calculation continues to use experimental data in this region instead of an HF calculation. In contrast to the situation with the ^{22}Ne(α, n)^{25}Mg reaction rate, this results in a significantly smaller ^{22}Ne(α, γ)^{26}Mg reaction rate at higher temperatures. Also, in contrast to [29], a much larger uncertainty is adopted based on direct comparison of the HF calculations to this higher energy data.

6.2 ^{22}Ne(α, γ)^{26}Mg at temperatures $\lesssim$ 1 GK

The rate for the ^{22}Ne(α, γ)^{26}Mg reaction for the lower temperature range of stellar helium burning environments was calculated using the narrow resonance formalism based on Eq. (3). The strengths of the lower energy resonances, which have not been directly observed, have been calculated from the partial widths given in Table 2 as described in the previous section. No direct measurements of the strengths of the low-energy resonances are available. Over much of the temperature range from 0.25 to 2.0 GK, the present rate is very similar to that of [29], but systematically lower by about 15%.

At temperatures below 0.25 GK, the present rate is dominated by the narrow resonance at $E_{c.m.}$ = 336 keV. This resonance, whose strength is based on the work of [23], was not included in the calculation by [29], which were performed prior to that experiment. Thus a substantially increased rate is obtained at these lower temperatures. A recent attempt of the LUNA collaboration [50] to directly measure the resonance strength yielded an experimental upper limit for the resonance strength, which however, would translate into a α spectroscopic factor, which is much larger than the allowed by the Wigner limit. The reaction rate is compared to that of [29] in Fig. 6.

7 Conclusion

With this paper, we have tried to elucidate the impact of nuclear structure configurations in the high excitation range

of the ^{26}Mg compound nucleus on the resonance contributions and strengths in the ^{22}Ne+α reaction processes. These configurations emerge in the vicinity of the α threshold at S_α = 10.61474(3) MeV and the neutron threshold S_n = 11.09309(4) MeV due to the collectivization of single-particle shell model states forming pronounced α-cluster configurations in an open many body quantum system. These α-cluster states dominate the reaction rates for both the ^{22}Ne(α, n)^{25}Mg and the ^{22}Ne(α, γ)^{26}Mg reaction channels with the respective resonance strengths depending on the single-particle components in the associated wave functions. These quantum effects determine the overall reaction rates, which therefore need to be considered in the framework of single-level considerations based on the R-matrix approach, taking all these parameters into account, rather than random statistical consideration of the Hauser-Feshbach model.

Acknowledgements This work was supported by the National Science Foundation through Grant no. Phys-0758100, and the Joint Institute for Nuclear Astrophysics through Grant No. Phys-0822648 and PHY-1430152 (JINA Center for the Evolution of the Elements). One of the authors, M.W., is also supported as a Wolfson Fellow of the British Royal Society. This research utilized the Notre Dame Center for Research Computing.

Data availability statement This manuscript has associated data in a data repository. [Authors' comment: No new data is reported in this work. All data shown in this work were obtained from the EXFOR database.]

References

1. M. Heil, R. Detwiler, R.E. Azuma, A. Couture, J. Daly, J. Görres, F. Käppeler, R. Reifarth, P. Tischhauser, C. Ugalde, M. Wiescher, Phys. Rev. C **78**, 025803 (2008). https://doi.org/10.1103/PhysRevC.78.025803
2. S. Bisterzo, R. Gallino, F. Käppeler, M. Wiescher, G. Imbriani, O. Straniero, S. Cristallo, J. Görres, R.J. de Boer, Mon. Not. R. Astron. Soc. **449**(1), 506 (2015). https://doi.org/10.1093/mnras/stv271
3. G.F. Ciani, L. Csedreki, D. Rapagnani, M. Aliotta, J. Balibrea-Correa, F. Barile, D. Bemmerer, A. Best, A. Boeltzig, C. Broggini, C.G. Bruno, A. Caciolli, F. Cavanna, T. Chillery, P. Colombetti, P. Corvisiero, S. Cristallo, T. Davinson, R. Depalo, A. Di Leva, Z. Elekes, F. Ferraro, E. Fiore, A. Formicola, Z. Fülöp, G. Gervino, A. Guglielmetti, C. Gustavino, G. Gyürky, G. Imbriani, M. Junker, M. Lugaro, P. Marigo, E. Masha, R. Menegazzo, V. Mossa, F.R. Pantaleo, V. Paticchio, R. Perrino, D. Piatti, P. Prati, L. Schiavulli, K. Stöckel, O. Straniero, T. Szücs, M.P. Takács, F. Terrasi, D. Vescovi, S. Zavatarelli, Phys. Rev. Lett. **127**, 152701 (2021). https://doi.org/10.1103/PhysRevLett.127.152701
4. M. Pignatari, R. Gallino, M. Heil, M. Wiescher, F. Käppeler, F. Herwig, S. Bisterzo, Astrophys. J. **710**(2), 1557 (2010). https://doi.org/10.1088/0004-637x/710/2/1557
5. J.B. Blake, D.N. Schramm, APJ **209**, 846 (1976). https://doi.org/10.1086/154782
6. F. Käppeler, M. Wiescher, U. Giesen, J. Görres, I. Baraffe, M. El Eid, C.M. Raiteri, M. Busso, R. Gallino, M. Limongi, A. Chieffi, Astrophys. J. **437**, 396 (1994). https://doi.org/10.1086/175004. https://ui.adsabs.harvard.edu/abs/1994ApJ...437..396K
7. J. Görres, C. Arlandini, U. Giesen, M. Heil, F. Käppeler, H. Leiste, E. Stech, M. Wiescher, Phys. Rev. C **62**, 055801 (2000). https://doi.org/10.1103/PhysRevC.62.055801
8. H. Trautvetter, M. Wiescher, K.U. Kettner, C. Rolfs, J. Hammer, Nucl. Phys. A **297**(3), 489 (1978). https://doi.org/10.1016/0375-9474(78)90156-2, https://www.sciencedirect.com/science/article/pii/0375947478901562
9. R.B. Vogelaar, T.R. Wang, S.E. Kellogg, R.W. Kavanagh, Phys. Rev. C **42**, 753 (1990). https://doi.org/10.1103/PhysRevC.42.753
10. S. Dababneh, M. Heil, F. Käppeler, J. Görres, M. Wiescher, R. Reifarth, H. Leiste, Phys. Rev. C **68**, 025801 (2003). https://doi.org/10.1103/PhysRevC.68.025801
11. A.C. Dombos, D. Robertson, A. Simon, T. Kadlecek, M. Hanhardt, J. Görres, M. Couder, R. Kelmar, O. Olivas-Gomez, E. Stech, F. Strieder, M. Wiescher, Phys. Rev. Lett. **128**, 162701 (2022). https://doi.org/10.1103/PhysRevLett.128.162701
12. D. Ashery, Nucl. Phys. A **136**(3), 481 (1969). https://doi.org/10.1016/0375-9474(69)90122-5, https://www.sciencedirect.com/science/article/pii/0375947469901225
13. F.X. Haas, J.K. Bair, Phys. Rev. C **7**, 2432 (1973). https://doi.org/10.1103/PhysRevC.7.2432
14. K. Wolke, V. Harms, H.W. Becker, J.W. Hammer, K.L. Kratz, C. Rolfs, U. Schröder, H.P. Trautvetter, M. Wiescher, A. Wöhr, Z. Phys. A **334**, 491–510 (1989). https://doi.org/10.1007/BF01294757
15. V. Harms, K.L. Kratz, M. Wiescher, Phys. Rev. C **43**, 2849 (1991). https://doi.org/10.1103/PhysRevC.43.2849
16. H.W. Drotleff, A. Denker, J.W. Hammer, H. Knee, S. Küchler, D. Streit, C. Rolfs, H.P. Trautvetter, Z. Phys. A **338**, 367–368 (1991). https://doi.org/10.1007/BF01288203
17. M. Jaeger, R. Kunz, A. Mayer, J.W. Hammer, G. Staudt, K.L. Kratz, B. Pfeiffer, Phys. Rev. Lett. **87**, 202501 (2001). https://doi.org/10.1103/PhysRevLett.87.202501
18. S. Hunt, C. Iliadis, A. Champagne, L. Downen, A. Cooper, Phys. Rev. C **99**, 045804 (2019). https://doi.org/10.1103/PhysRevC.99.045804
19. C. Massimi, S. Altstadt, J. Andrzejewski, L. Audouin, M. Barbagallo, V. Bàcares, F. Bevâr, F. Belloni, E. Berthoumieux, J. Billowes, S. Bisterzo, D. Bosnar, M. Brugger, M. Calviani, F. Calviño, D. Cano-Ott, C. Carrapiço, D. Castelluccio, F. Cerutti, E. Chiaveri, L. Cosentino, M. Chin, G. Clai, N. Colonna, G. Cortés, M. Cortés-Giraldo, S. Cristallo, M. Diakaki, C. Domingo-Pardo, I. Duran, R. Dressler, C. Eleftheriadis, A. Ferrari, P. Finocchiaro, K. Fraval, S. Ganesan, A. García, G. Giubrone, I. Gonçalves, E. González-Romero, E. Griesmayer, C. Guerrero, F. Gunsing, A. Hernández-Prieto, D. Jenkins, E. Jericha, Y. Kadi, F. Käppeler, D. Karadimos, N. Kivel, P. Koehler, M. Kokkoris, S. Kopecky, M. Krtička, J. Kroll, C. Lampoudis, C. Langer, E. Leal-Cidoncha, C. Lederer, H. Leeb, L. Leong, S.L. Meo, R. Losito, A. Mallick, A. Manousos, J. Marganiec, T. Martínez, P. Mastinu, M. Mastromarco, E. Mendoza, A. Mengoni, P. Milazzo, F. Mingrone, M. Mirea, W. Mondelaers, A. Musumarra, C. Paradela, A. Pavlik, J. Perkowski, M. Pignatari, L. Piersanti, A. Plom-

pen, J. Praena, J. Quesada, T. Rauscher, R. Reifarth, A. Riego, M. Robles, C. Rubbia, M. Sabaté-Gilarte, R. Sarmento, A. Saxena, P. Schillebeeckx, S. Schmidt, D. Schumann, G. Tagliente, J. Tain, D. Tarrío, L. Tassan-Got, A. Tsinganis, S. Valenta, G. Vannini, I.V. Rijs, V. Variale, P. Vaz, A. Ventura, M. Vermeulen, V. Vlachoudis, R. Vlastou, A. Wallner, T. Ware, M. Weigand, C. Weiβ, R. Wynants, T. Wright, P. Žugec, Phys. Lett. B **768**, 1 (2017). https://doi.org/10.1016/j.physletb.2017.02.025, http://www.sciencedirect.com/science/article/pii/S0370269317301260

20. C. Massimi, P. Koehler, S. Bisterzo, N. Colonna, R. Gallino, F. Gunsing, F. Käppeler, G. Lorusso, A. Mengoni, M. Pignatari, G. Vannini, U. Abbondanno, G. Aerts, H. Álvarez, F. Álvarez-Velarde, S. Andriamonje, J. Andrzejewski, P. Assimakopoulos, L. Audouin, G. Badurek, M. Barbagallo, P. Baumann, F. Bečvář, F. Belloni, M. Bennett, E. Berthoumieux, M. Calviani, F. Calviño, D. Cano-Ott, R. Capote, C. Carrapiço, A. Carrillo de Albornoz, P. Cennini, V. Chepel, E. Chiaveri, G. Cortes, A. Couture, J. Cox, M. Dahlfors, S. David, I. Dillmann, R. Dolfini, C. Domingo-Pardo, W. Dridi, I. Duran, C. Eleftheriadis, M. Embid-Segura, L. Ferrant, A. Ferrari, R. Ferreira-Marques, L. Fitzpatrick, H. Frais-Koelbl, K. Fujii, W. Furman, I. Goncalves, E. González-Romero, A. Goverdovski, F. Gramegna, E. Griesmayer, C. Guerrero, B. Haas, R. Haight, M. Heil, A. Herrera-Martinez, F. Herwig, R. Hirschi, M. Igashira, S. Isaev, E. Jericha, Y. Kadi, D. Karadimos, D. Karamanis, M. Kerveno, V. Ketlerov, V. Konovalov, S. Kopecky, E. Kossionides, M. Krtička, C. Lampoudis, H. Leeb, C. Lederer, A. Lindote, I. Lopes, R. Losito, M. Lozano, S. Lukic, J. Marganiec, L. Marques, S. Marrone, T. Martínez, P. Mastinu, E. Mendoza, P.M. Milazzo, C. Moreau, M. Mosconi, F. Neves, H. Oberhummer, S. O'Brien, M. Oshima, J. Pancin, C. Papachristodoulou, C. Papadopoulos, C. Paradela, N. Patronis, A. Pavlik, P. Pavlopoulos, L. Perrot, M.T. Pigni, R. Plag, A. Plompen, A. Plukis, A. Poch, J. Praena, C. Pretel, J. Quesada, T. Rauscher, R. Reifarth, G. Rockefeller, M. Rosetti, C. Rubbia, G. Rudolf, J. Salgado, C. Santos, L. Sarchiapone, R. Sarmento, I. Savvidis, C. Stephan, G. Tagliente, J.L. Tain, D. Tarrío, L. Tassan-Got, L. Tavora, R. Terlizzi, P. Vaz, A. Ventura, D. Villamarin, V. Vlachoudis, R. Vlastou, F. Voss, S. Walter, H. Wendler, M. Wiescher, K. Wisshak, Phys. Rev. C **85**, 044615 (2012). https://doi.org/10.1103/PhysRevC.85.044615
21. U. Giesen, C. Browne, J. Görres, S. Graff, C. Iliadis, H.P. Trautvetter, M. Wiescher, W. Harms, K. Kratz, B. Pfeiffer, R. Azuma, M. Buckby, J. King, Nucl. Phys. A **561**(1), 95 (1993). https://doi.org/10.1016/0375-9474(93)90167-V, https://www.sciencedirect.com/science/article/pii/037594749390167V
22. C. Ugalde, A.E. Champagne, S. Daigle, C. Iliadis, R. Longland, J.R. Newton, E. Osenbaugh-Stewart, J.A. Clark, C. Deibel, A. Parikh, P.D. Parker, C. Wrede, Phys. Rev. C **76**, 025802 (2007). https://doi.org/10.1103/PhysRevC.76.025802
23. R. Talwar, T. Adachi, G.P.A. Berg, L. Bin, S. Bisterzo, M. Couder, R.J. Boer, X. Fang, H. Fujita, Y. Fujita, J. Görres, K. Hatanaka, T. Itoh, T. Kadoya, A. Long, K. Miki, D. Patel, M. Pignatari, Y. Shimbara, A. Tamii, M. Wiescher, T. Yamamoto, M. Yosoi, Phys. Rev. C **93**, 055803 (2016). https://doi.org/10.1103/PhysRevC.93.055803
24. H. Jayatissa, G. Rogachev, V. Goldberg, E. Koshchiy, G. Christian, J. Hooker, S. Ota, B. Roeder, A. Saastamoinen, O. Trippella, S. Upadhyayula, E. Uberseder, Phys. Lett. B **802**, 135267 (2020). https://doi.org/10.1016/j.physletb.2020.135267, https://www.sciencedirect.com/science/article/pii/S037026932030071X
25. S. Ota, G. Christian, G. Lotay, W. Catford, E. Bennett, S. Dede, D. Doherty, S. Hallam, J. Hooker, C. Hunt, H. Jayatissa, A. Matta, M. Moukaddam, G. Rogachev, A. Saastamoinen, J. Tostevin, S. Upadhyayula, R. Wilkinson, Phys. Lett. B **802**, 135256 (2020). https://doi.org/10.1016/j.physletb.2020.135256, https://www.sciencedirect.com/science/article/pii/S0370269320300605
26. S. Ota, G. Christian, W.N. Catford, G. Lotay, M. Pignatari, U. Battino, E.A. Bennett, S. Dede, D.T. Doherty, S. Hallam, F. Herwig, J. Hooker, C. Hunt, H. Jayatissa, A. Matta, M. Moukaddam, E. Rao, G.V. Rogachev, A. Saastamoinen, D. Scriven, J.A. Tostevin, S. Upadhyayula, R. Wilkinson, Phys. Rev. C **104**, 055806 (2021). https://doi.org/10.1103/PhysRevC.104.055806
27. G. Lotay, D.T. Doherty, D. Seweryniak, S. Almaraz-Calderon, M.P. Carpenter, C.J. Chiara, H.M. David, C.R. Hoffman, R.V.F. Janssens, A. Kankainen, T. Lauritsen, R. Wilkinson, P.J. Woods, S. Zhu, Eur. Phys. J. A **55**, 109 (2019). https://doi.org/10.1140/epja/i2019-12791-5
28. P.E. Koehler, Phys. Rev. C **66**, 055805 (2002). https://doi.org/10.1103/PhysRevC.66.055805
29. R. Longland, C. Iliadis, A.I. Karakas, Phys. Rev. C **85**, 065809 (2012). https://doi.org/10.1103/PhysRevC.85.065809
30. P. Adsley, U. Battino, A. Best, A. Caciolli, A. Guglielmetti, G. Imbriani, H. Jayatissa, M. La Cognata, L. Lamia, E. Masha, C. Massimi, S. Palmerini, A. Tattersall, R. Hirschi, Phys. Rev. C **103**, 015805 (2021). https://doi.org/10.1103/PhysRevC.103.015805
31. W.A. Fowler, G.R. Caughlan, B.A. Zimmerman, Ann. Rev. Astron. Astrophys. **13**(1), 69 (1975). https://doi.org/10.1146/annurev.aa.13.090175.000441
32. T. Rauscher, F.K. Thielemann, J. Görres, M. Wiescher, Nucl. Phys. A **675**(3), 695 (2000). https://doi.org/10.1016/S0375-9474(00)00182-2, https://www.sciencedirect.com/science/article/pii/S0375947400001822
33. K. Ikeda, N. Takigawa, H. Horiuchi, Prog. Theor. Phys. Suppl. **E68**, 464 (1968). https://doi.org/10.1143/PTPS.E68.464
34. J. Okołowicz, W. Nazarewicz, M. Płoszajczak, Fortschr. Phys. **61**(2–3), 66 (2013). https://doi.org/10.1002/prop.201200127
35. P. Adsley, J.W. Brümmer, T. Faestermann, S.P. Fox, F. Hammache, R. Hertenberger, A. Meyer, R. Neveling, D. Seiler, N. de Séréville, H.F. Wirth, Phys. Rev. C **97**, 045807 (2018). https://doi.org/10.1103/PhysRevC.97.045807
36. Y. Chen, G.P.A. Berg, R.J. deBoer, J. Görres, H. Jung, A. Long, K. Seetedohnia, R. Talwar, M. Wiescher, S. Adachi, H. Fujita, Y. Fujita, K. Hatanaka, C. Iwamoto, B. Liu, S. Noji, H.J. Ong, A. Tamii, Phys. Rev. C **103**, 035809 (2021). https://doi.org/10.1103/PhysRevC.103.035809
37. Y. Chen, Study of high energy levels in ^{26}Mg through the (d, p) reaction and it's implications for the neutron source in nuclear astrophysics. Ph.D. thesis, University of Notre Dame (2019)
38. P. Adsley, J.W. Brümmer, K.C.W. Li, D.J. Marín-Lámbarri, N.Y. Kheswa, L.M. Donaldson, R. Neveling, P. Papka, L. Pellegri, V. Pesudo, L.C. Pool, F.D. Smit, J.J. van Zyl, Phys. Rev. C **96**, 055802 (2017). https://doi.org/10.1103/PhysRevC.96.055802
39. R. Longland, C. Iliadis, G. Rusev, A.P. Tonchev, R.J. Boer, J. Görres, M. Wiescher, Phys. Rev. C **80**, 055803 (2009). https://doi.org/10.1103/PhysRevC.80.055803
40. M. Jaeger, Die Einfangreaktion ^{22}Ne$(\alpha, \gamma)^{26}$Mg - die Hauptneutronenquelle in massiven Sternen. Ph.D. thesis, Institut für Strahlenphysik der Universität Stuttgart (2001)
41. J. Shahina, D. Görres, M. Robertson, O. Couder, A. Gomez, M. Gula, T. Hanhardt, R. Kadlecek, P. Kelmar, A. Scholz, E. Simon, F. Stech, M. Strieder, Wiescher. Phys. Rev. C **106**, 025805 (2022). https://doi.org/10.1103/PhysRevC.106.025805
42. M. Beard, E. Uberseder, R. Crowter, M. Wiescher, Phys. Rev. C **90**, 034619 (2014). https://doi.org/10.1103/PhysRevC.90.034619
43. W.A. Peters, Phys. Rev. C **96**, 029801 (2017). https://doi.org/10.1103/PhysRevC.96.029801
44. R.E. Azuma, E. Uberseder, E.C. Simpson, C.R. Brune, H. Costantini, R.J. de Boer, J. Görres, M. Heil, P.J. LeBlanc, C. Ugalde, M. Wiescher, Phys. Rev. C **81**, 045805 (2010). https://doi.org/10.1103/PhysRevC.81.045805

45. E. Uberseder, R.J. deBoer, AZURE2 User Manual (2015). http://www.azure.nd.edu
46. J.R. Newton, R. Longland, C. Iliadis, Phys. Rev. C **78**, 025805 (2008). https://doi.org/10.1103/PhysRevC.78.025805
47. W. Huang, M. Wang, F. Kondev, G. Audi, S. Naimi, Chin. Phys. C **45**(3), 030002 (2021). https://doi.org/10.1088/1674-1137/abddb0
48. M. Wang, W. Huang, F. Kondev, G. Audi, S. Naimi, Chin. Phys. C **45**(3), 030003 (2021). https://doi.org/10.1088/1674-1137/abddaf
49. E. Kuhlmann, E. Ventura, J.R. Calarco, D.G. Mavis, S.S. Hanna, Phys. Rev. C **11**, 1525 (1975). https://doi.org/10.1103/PhysRevC.11.1525
50. D. Piatti, E. Masha, M. Aliotta, J. Balibrea-Correa, F. Barile, D. Bemmerer, A. Best, A. Boeltzig, C. Broggini, C.G. Bruno, A. Caciolli, F. Cavanna, T. Chillery, G.F. Ciani, A. Compagnucci, P. Corvisiero, L. Csedreki, T. Davinson, R. Depalo, A. di Leva, Z. Elekes, F. Ferraro, E.M. Fiore, A. Formicola, Z. Fülöp, G. Gervino, A. Guglielmetti, C. Gustavino, G.IGy. Gyürky, M. Junker, M. Lugaro, P. Marigo, R. Menegazzo, V. Mossa, F.R. Pantaleo, V. Paticchio, R. Perrino, P. Prati, D. Rapagnani, L. Schiavulli, J. Skowronski, K. Stöckel, O. Straniero, T. Szücs, M.P. Takács, S. Zavatarelli, Eur. Phys. J. A **58**, 194 (2022). https://doi.org/10.1140/epja/s10050-022-00827-2